Changes in Ni-NiO Equilibrium Due to $LaFeO_3$ and the Effect on Dry Reforming of CH_4

Xinyu Mao[a], Alexandre C. Foucher[b], Eric A. Stach[b] and Raymond J. Gorte[a,b]*

[a] Department of Chemical and Biomolecular Engineering, University of Pennsylvania, Philadelphia, PA 19104, USA.

[b] Department of Materials Science and Engineering, University of Pennsylvania, Philadelphia, PA 19104, USA.

*Corresponding Author: **gorte@seas.upenn.edu,** orcid.org/0000-0003-0879-715X

Abstract:

The interactions between Ni and $LaFeO_3$ were studied on catalysts prepared by Atomic Layer Deposition (ALD) of 0.5-nm films of $LaFeO_3$ on $MgAl_2O_4$. Scanning Transmission Electron Microscopy showed that the films covered the support uniformly, even after 5 redox cycles at 1073 K, and X-Ray Diffraction showed that the films had the perovskite structure. Equilibrium between Ni and NiO was studied using coulometric-titration and flow-titration measurements on 5-wt% Ni catalysts, with and without $LaFeO_3$. While equilibrium constants for $Ni/MgAl_2O_4$ were similar to that expected for bulk Ni, equilibrium P_{O_2} were shifted to significantly lower values in the presence of $LaFeO_3$. In studies of Methane Dry Reforming, the shift in equilibrium resulted in catalyst deactivation due to Ni oxidation at low $CO:CO_2$ ratios, even though $Ni/LaFeO_3/MgAl_2O_4$ otherwise showed a high reaction rate and excellent tolerance against coking.

KEYWORDS

Ni-NiO equilibrium; $LaFeO_3$; Methane Dry Reforming; Atomic Layer Deposition (ALD); "Intelligent" catalysts.

1. Introduction

The reversible incorporation of transition-metal catalysts into perovskite lattices has been receiving an increasing amount of attention, both for heterogeneous catalysts [1-3] and as fuel electrodes in Solid Oxide Fuel Cells (SOFC) [4, 5]. The original goal behind these "Intelligent" catalysts was to restore lost metal dispersion by incorporating the metal atoms into the lattice during high-temperature oxidation, then ex-solving the metal atoms back to the surface by high-temperature reduction [1, 6, 7]. However, a number of recent studies have shown that these perovskite-supported metals may also have other favorable properties. In particular, perovskite-supported Ni catalysts appear to show good activity for reforming of methane [8, 9], while showing outstanding stability against coking [2, 10]. Since this has been observed for a number of different perovskites (e.g. $BaZrO_3$ [11], $LaMnO_3$ [12], and doped $SrTiO_3$ [13]), the anti-coking phenomenon appears to be very general.

For catalytic applications, one factor preventing the implementation of perovskite-supported metals is that most perovskites exist in the form of relatively large crystallites after typical pretreatments. This has two important implications. First, the formation of large crystallites implies that the catalysts formed from these supports will have low surface areas. Second, and more importantly, it has been shown that much of the ex-solved catalytic metal remains in the bulk of the perovskite and is unavailable for reaction [2, 14, 15]. Therefore, to achieve higher surface areas and reduce the length scale for any ingress-egress of metal particles, our group has been preparing thin-film perovskites on high-surface-area supports using Atomic Layer Deposition. The preparation of 1-nm $CaTiO_3$ [10] and $LaFeO_3$ [16] films on $MgAl_2O_4$ substrates has been demonstrated. While questions remain about whether films that are thinner than a typical metal-catalyst particle size can show true ex-solution behavior, catalysts prepared

from these thin-film supports do show similar characteristics with catalysts prepared from bulk perovskites, including loss of catalytic activity upon high-temperature calcination and restoration of that activity upon high-temperature reduction [10, 16].

An interesting question arises regarding the thermodynamics of metal oxidation and reduction when the metal is supported on a strongly interacting support. With Ni, for example, the thermodynamics of oxidation are normally described by the reaction, $Ni + ½O_2 = NiO$, for which the equilibrium constant, K_{NiO}, is equal to $P_{O_2}^{-½}$. K_{NiO} is determined from ΔG of the oxidation reaction. If the Ni^{2+} ions exist in a perovskite lattice, rather than as bulk NiO, or even if the NiO phase interacts strongly with the support, the equilibrium constant for this reaction could be affected [17]. This has very practical implications. In practice, the P_{O_2} is established by equilibrium with either H_2 and H_2O or CO and CO_2; and, at high H_2O:H_2 ratios and lower temperatures, the metal can be oxidized. This has been discussed as a potential problem for Co-based Fischer-Tropsch catalysts [18]. It is also important with Ni-based anodes in Solid Oxide Fuel Cells, since oxidation of Ni can occur at high fuel utilizations and lower temperatures [19].

Carbon whisker formation is a major problem with Ni catalysts used in methane-reforming reactions, and much effort has gone into developing ways to limit this carbon. For example, it is known that precious metals, e.g. Pt, Rh and Pd, exhibit significantly better tolerance against carbon deposition [20, 21]; however, due to the high cost, most research has focused on modifying Ni catalysts. It has been reported that basic oxides, such as CaO or La-containing materials [22-24], also improve stability against coking. However, perovskite-based supports appear to modify Ni in ways that are different from that of the individual oxides due to the fact that Ni can, under some conditions, reversibly enter the perovskite lattice [2, 10].

Here, we present results from a thermodynamic and catalytic investigation of Ni on thin $LaFeO_3$ films. The presence of $LaFeO_3$ is found to shift the equilibrium constant to significantly lower P_{O_2}, which in turn affects the conditions under which Ni can be used as a steam-reforming catalyst.

2. Experimental Methods

2.1 Sample Preparation

The $MgAl_2O_4$ support used in this study was prepared in our laboratory using co-precipitation of magnesium nitrate hexahydrate (Sigma-Aldrich, USA) and aluminum nitrate nonahydrate (Sigma-Aldrich, USA). The resulting precipitates were rinsed with distilled water, dried in the oven for 3 h, and calcined in a muffle furnace at 1173 K overnight. The sample was then washed in concentrated HNO_3 (Fisher Scientific, USA) to remove any excess MgO and Al_2O_3. After this treatment, the final product had a BET surface area of 120 m^2/g and an X-Ray Diffraction (XRD) pattern that showed only characteristic peaks of $MgAl_2O_4$.

The $LaFeO_3$ films were deposited onto the $MgAl_2O_4$ support by ALD using a home-built, static system that has been described in more detail elsewhere [25]. The ALD precursors were $La(TMHD)_3$ (TMHD = 2,2,6,6-tetramethyl-3,5-heptanedionato, Strem Chemicals, Inc.) and ferrocene ($Fe(Cp)_2$, Sigma-Aldrich). During the deposition process, the evacuated $MgAl_2O_4$ substrate was exposed to 5 Torr of one of the precursor vapors at 523 K for 5 min, after which the sample was evacuated. The oxidation part of an ALD cycle for $Fe(Cp)_2$ was carried out inside the system using oxygen at 523 K, while $La(TMHD)_3$ was oxidized in a muffle furnace at 873 K for 1 min to fully remove the TMHD ligands. Growth rates for each oxide were determined by measuring the sample weight after every 5 ALD cycles and were found to be to be $3.4x10^{13}$ La/cm^2-cycle (0.017 nm La_2O_3/cycle, assuming the films had the same density as the bulk) and $1x10^{14}$ Fe/cm^2-cycle (0.030 nm Fe_2O_3/cycle). To prepare $LaFeO_3$ films, we alternated between 3 cycles of La and 1 cycle of Fe in order to produce a sample with the correct stoichiometry. The final loading was chosen to be 30-wt% $LaFeO_3$, which corresponds to an average perovskite film thickness of 0.5 nm.

To ensure that there was good initial contact with the supports, Ni was added by ALD. The precursor was $Ni(TMHD)_2$ (Strem Chemicals, Inc.), and the procedures were essentially the same as those used to deposit La_2O_3. The number of ALD cycles was varied in order to achieve a final Ni loading of approximately 1.0-wt% or 5.0-wt%. After deposition, the $Ni/LaFeO_3/MgAl_2O_4$ was alternately oxidized for 30 min in 10% O_2-He mixtures and reduced in 10% H_2-He mixtures for 30 min five times at 1073 K before acquiring data in order to crystallize the $LaFeO_3$ films.

2.2 Characterization Methods

XRD was performed using a Rigaku MiniFlex diffractometer equipped with a Cu Kα source (λ = 0.15406 nm). Specific surface areas were determined from BET isotherms with N_2 at 78 K using home-built equipment. Scanning Transmission Electron Microscopy (STEM) and Energy Dispersive X-ray Spectra (EDS) were performed with a JEOL JEM-F200 STEM, operated at 200 kV. Powder specimens for STEM characterization were diluted in methanol and put on lacey carbon films on copper grids (Electron Microscopy Sciences). The loading of Ni on each sample was measured using Inductively Coupled Plasma-Optical Emission Spectrometry (ICP-OES), equipped with a Mod Lichte nebulizer. CO and H_2 chemisorption measurements were attempted; however, as reported in previous studies with perovskite-supported catalysts [10], we were not able to see significant adsorption uptakes.

Equilibrium measurements were performed using either flow-titration or coulometric titration [26, 27], depending on the range of P_{O_2} at which oxidation of the catalyst took place. In flow titration, the samples were first allowed to come to equilibrium at a given P_{O_2}, established by exposure to a fixed H_2-H_2O mixture and assuming the H_2 oxidation reaction, $H_2 + ½O_2 = H_2O$, reaches equilibrium. The average oxidation state of the catalyst at that P_{O_2} was then

determined by measuring the amount of oxygen required to fully oxidize the sample. The flow-titration experiments were performed by placing 0.5-g samples in flow reactor, reducing the catalyst in dry H_2 for 30 min, and then equilibrating the catalyst in a flowing H_2-H_2O mixture (20 mL/min) for another 30 min. The partial pressure of H_2O in the H_2-H_2O mixture was controlled by the temperature of a water bubbler through which the H_2 passed. After purging the reactor with dry He, the sample was exposed to dry, flowing air (10 mL/min) while monitoring the effluent products using a quadrupole mass spectrometer (SRS RGA-100). The amount of oxygen required to re-oxidize the sample could be calculated by integrating the difference between N_2 and O_2 signals. It is important to point out that equilibrium in the flow-titration measurements was approached starting from the reduced sample, implying that Ni oxidation occurs in the H_2-H_2O mixture and is not limited by the kinetics of reduction.

Because there is a limited range of H_2:H_2O ratios that can be accurately measured in a flow system, coulometric titration was used for thermodynamic measurements on samples requiring higher P_{O_2} for oxidation [26]. In coulometric titration, 0.5-g samples were placed in the center of a YSZ (yttria-stabilized zirconia, 1-cm diameter, 30-cm long) tube which had Ag electrodes painted on both inside and outside. After placing the YSZ tube in a horizontal tube furnace, the center of the tube with the sample was heated to 1073 K at a heating rate of 1.0 K/min. The sample was then pretreated with flowing gases, either a mixture of 5% H_2O, 10% H_2, and 85% He for experiments that started with a reduced sample or a mixture of 5% H_2O, 10% O_2, and 85% He for measurements starting with an oxidized sample. After the sample had equilibrated, the ends of the YSZ tube were sealed with Cajon fittings. Known quantities of oxygen were then electrochemically pumped into or out of the YSZ tube by applying a known charge across the electrodes using a Gamry instruments potentiostat. After allowing the system

to come to equilibrium with the electrodes at open circuit, the equilibrium P_{O_2} could be calculated from the open circuit potential across the Ag electrodes using the Nernst Equation.

Steady-state, Methane-Dry-Reforming (MDR) rates were performed over the Ni catalysts using 0.1-g samples in a 1/4-inch, quartz, tubular flow reactor. Estimates of the Peclet number in the system suggest that flow in the tubular reactors is sufficiently well mixed so that CSTR conditions may be assumed [28]. Products were detected with an on-line gas chromatograph (SRI8610C) equipped with a Hayesep Q column and a TCD detector. Initially, the reactions on both $Ni/MgAl_2O_4$ and $Ni/LaFeO_3/MgAl_2O_4$ were measured as a function of temperature using 5% each of CH_4 and CO_2 in He, with a total gas flow rate of 100 mL/min. The MDR reaction on $Ni/LaFeO_3/MgAl_2O_4$ was also studied as a function of the CH_4:CO_2 ratio, with the total flow rate again fixed at 100 mL/min. Before acquiring rate data, all Ni catalysts were reduced in a 10% H_2-He mixture.

Coking tests were performed by flowing 10% CH_4-He mixtures, with a total flow rate of 100 mL/min, over 0.1-g catalyst samples for 12 h at 1073 K. The carbon contents of the catalysts were then obtained from the amount of CO_2 formed during oxidation at 1073 K. Oxidation was carried out in 20% O_2-He mixtures, at a flow rate of 50 ml/min, using the quadrupole mass spectrometer to measure CO_2 production.

3. Results

3.1 Sample Characterization

A list of the samples used in this study is shown in Table 1, together with their BET surface areas and catalyst loadings. The lower surface areas of the $LaFeO_3$-containing samples are due mainly to the increased mass of the samples, with a small contribution from a decrease in pore size [16]. The $LaFeO_3$ loading was 30-wt% (±1.5-wt%) determined by weight-gain measurements, while Ni loadings for each sample were measured by ICP-OES with an uncertainty of ±0.1-wt%.

Table 1. Properties of samples used in the present study. The oxygen uptakes (and extent of Ni reduction) were measured at 1073 K on samples after the following pretreatments: reduction in dry H_2 at (1) 1073 K, reduction in dry H_2 at 1073 K followed by oxidation in dry air at (2) 973 K, (3) 873 K, and (4) 773 K.

	BET S.A. (± 3 m^2/g)	Ni loading (± 0.1%)	µmol O/g uptake (Ni reduction extent) (±20 µmol)			
			(1)	(2)	(3)	(4)
5-Ni/MAO	115	4.8	720 (88%)	0 (0%)	0 (0%)	50 (6%)
5-Ni/LFO/MAO	55	4.9	870 (100%)	90 (10%)	500 (57%)	760 (87%)
1-Ni/LFO/MAO	58	0.9	200 (100%)			
LFO/MAO	61	-	60 (-)			

Note: $MgAl_2O_4$ is abbreviated as MAO and $LaFeO_3$ as LFO.

XRD patterns for the oxidized and reduced 5-Ni/LFO/MAO and 5-Ni/MAO samples are shown in Figure 1. As discussed earlier, the diffraction patterns here were obtained on samples that had undergone five oxidation and reduction cycles at 1073 K in order to improve crystallization of the films. Results for 5-Ni/LFO/MAO are reported in Figure 1a), with the pattern for $MgAl_2O_4$ shown for comparison. Besides the peaks associated with $MgAl_2O_4$, the

dominant diffraction peaks on the 5-Ni/LFO/MAO sample after the five redox cycles were those associated with the perovskite phase. These features did not change significantly with oxidation or reduction; and an estimate of crystallite size based on the width of the peaks, using Scherrer's Equation, gave values between 9 and 12 nm. More significantly, the reduced sample showed small peaks at 44 and 51 degrees 2θ for metallic Ni, with a particle size of 10 nm. Compared to normal Ni, the peak positions for metallic Ni on 5-Ni/LFO/MAO were shifted 0.4 degrees to lower angles. This lattice expansion, from 352.4 pm to 355.3 pm, may be caused by weakening of Ni-Ni bonds due to strong interactions with $LaFeO_3$. The peaks due to Ni disappeared after oxidation but there were no observable NiO features. XRD patterns for 5-Ni/MAO, Figure 1b), show much more intense and narrower Ni features on the reduced sample, due to the presence of

larger Ni particles compared to those on $LaFeO_3$, and only $MgAl_2O_4$ peaks on the oxidized sample.

Figure 1. XRD patterns of (a) 5-Ni/LFO/MAO and (b) 5-Ni/MAO: (i) unmodified $MgAl_2O_4$; (ii) oxidized Ni-containing sample after 5 redox cycles at 1073 K; (iii) reduced Ni-containing sample after 5 redox cycles at 1073 K. Perovskite features are marked with stars, metallic Ni with 4-point stars.

STEM and EDS results for the oxidized and reduced 5-Ni/LFO/MAO sample are shown in Figure 2. The STEM image of the oxidized sample, Figure 2a), does not show any well-defined particles and the EDS elemental maps indicate that La, Fe, and Ni are present as a relatively uniform coating on the surface, although there is a region near the bottom of the image that may be Ni-rich. Despite the harsh redox cycling, there is no evidence that either the Ni or the

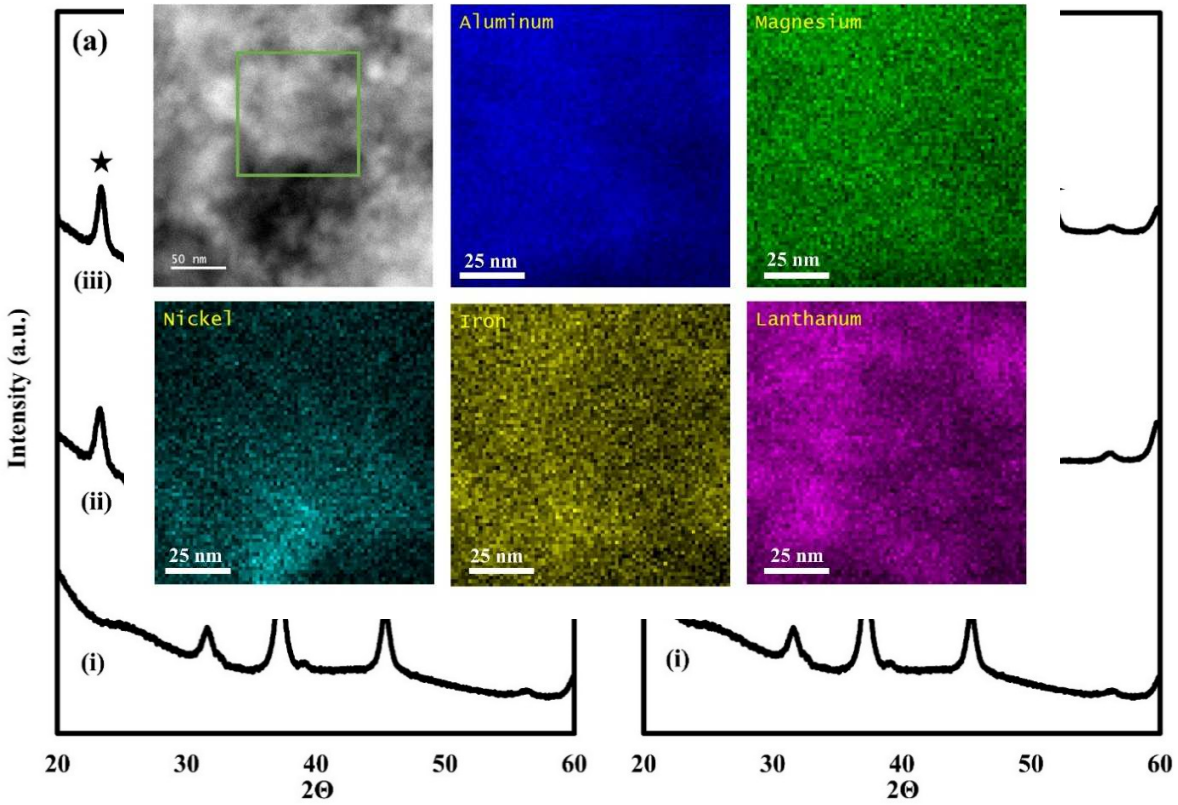

$LaFeO_3$ had agglomerated into large particles. For the reduced sample, there is some indication of Ni and $LaFeO_3$ agglomeration, shown in Figure 2b), although this may also be due to

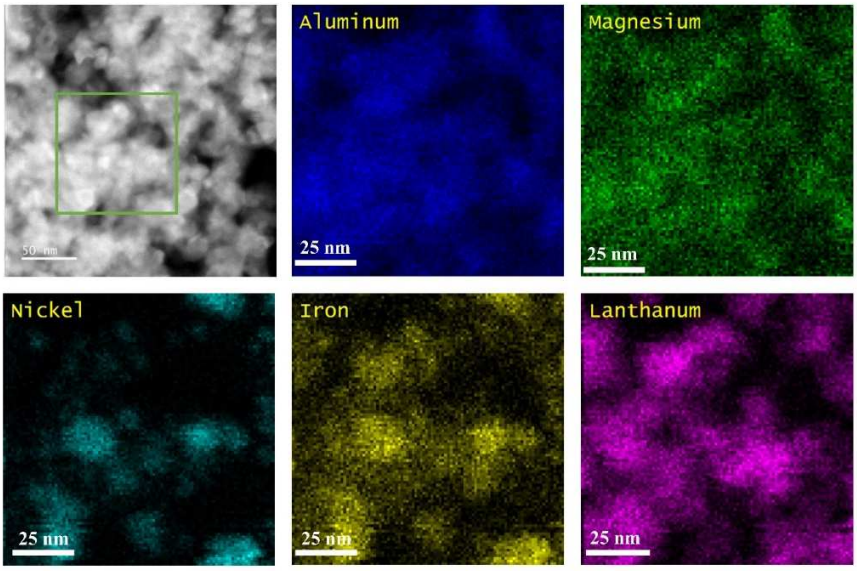

roughness in the sample. There is clearly overlap in the locations of Ni, La, and Fe. By contrast, the formation of distinct Ni particles is more obvious on reduced 5-Ni/MAO after the same treatment, as shown in Figure 2c).

Figure 2a). High angle annular dark field STEM image and EDS maps of Mg, Al, La, Fe and Ni on oxidized 5-Ni/LFO/MAO after 5 redox cycles, taken from the region indicated by the green box.

Figure 2b). High angle annular dark field STEM image and EDS maps of Mg, Al, La, Fe and Ni on reduced 5-Ni/LFO/MAO after 5 redox cycles, taken from the region indicated by the green box.

Figure 2c). High angle annular dark field STEM image and EDS map of Ni on reduced 5-Ni/MAO after 5 redox cycles, taken from the region indicated by the green box.

3.2 Thermodynamic Measurements

The total amount of oxygen that could be added or removed from the Ni-containing samples after reduction or oxidation at 1073 K was measured by flow titration and the values are listed in Table 1 (Column (1)). For these experiments, the samples were reduced in dry H_2 at 1073 K, after which the amount of O_2 required to completely oxidize the samples at 1073 K was measured. As expected, there was no reduction of $MgAl_2O_4$; but an uptake of ~60 µmol O/g on the reduced LFO/MAO was observed. This indicates that the reduced perovskite phase had a

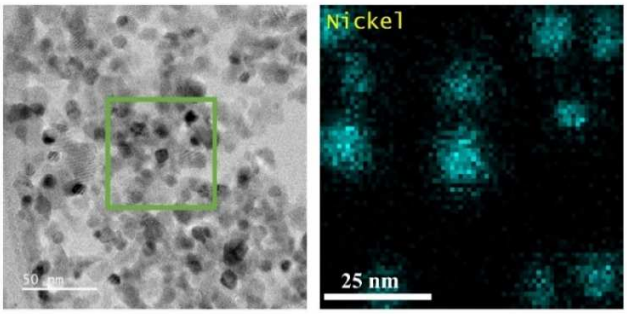

stoichiometry of $LaFeO_{2.985}$. Thermodynamic measurements of Sr-doped $LaFeO_3$ would suggest a similar reduction of Fe under these conditions [29]. By contrast, the oxygen uptakes on the reduced 5-Ni/MAO, 5-Ni/LFO/MAO, and 1-Ni/LFO/MAO, samples were 720, 870, and 200 µmol O/g, respectively. For samples with 0.9-, 4.8-, and 4.9-wt% Ni, the reaction of Ni to NiO would require 150, 820 and 830 µmol O/g, respectively. Therefore, the oxygen uptakes on the Ni/LFO/MAO samples are in reasonable agreement with those expected for oxidation of both the Ni and $LaFeO_3$ phases. The fact that oxygen uptakes increased proportionally with Ni content also excludes the possibility that Ni is catalyzing reduction of the perovskite. The somewhat

lower oxygen uptake on 5-Ni/MAO may indicate that some of the Ni had reacted with the $MgAl_2O_4$ and was unable to reduce back to the metallic state at these conditions.

In a previous investigation of $Pd/LaFeO_3/MgAl_2O_4$ [16], it was found that reduction or oxidation at temperatures below 1073 K was ineffective for activating or deactivating the catalyst. To explore the effect of pretreatment temperature on 5-Ni/LFO/MAO and 5-Ni/MAO, we measured the oxidation state of pre-reduced samples after oxidation at intermediate temperatures. The catalysts were first reduced at 1073 K, after which they were oxidized in dry air for 30 min at either 973, 873, or 773 K. The sample temperature was then raised to 1073 K and the oxidation state measured by flow titration. As shown by the data in Table 1 (Columns (2) to (4)), the 5-Ni/MAO catalyst could be fully oxidized at 773 K. By comparison, most of the Ni in the 5-Ni/LFO/MAO remained in the reduced state after oxidation at 773 K. Oxidation was incomplete even after heating in flowing air at 873 K. The increased difficulty of oxidizing the $LaFeO_3$-containing sample suggests that oxidation of the Ni involves some interaction with the perovskite.

To explore the chemical potential at which oxidation occurs, this work specifically investigated the thermodynamics of oxidation in these catalyst using equilibrium measurements. Data for the redox reaction on the 5-Ni/MAO catalyst at 1073 K are shown in Figure 3a). Because the Ni remained completely reduced for all H_2:H_2O ratios that we could access in the flow-titration apparatus, these measurements were performed by coulometric titration, starting from the reduced sample. After flowing a mixture of 5% H_2O, 10% H_2, and 85% He over the sample for 30 min and then allowing the system to come to equilibrium, the measured P_{O_2} was 10^{-16} atm. The P_{O_2} increased only slightly, from 10^{-16} atm to 10^{-15} atm, upon the addition of the first 700 µmol O/g to the sample but then increased rapidly after the Ni was completely

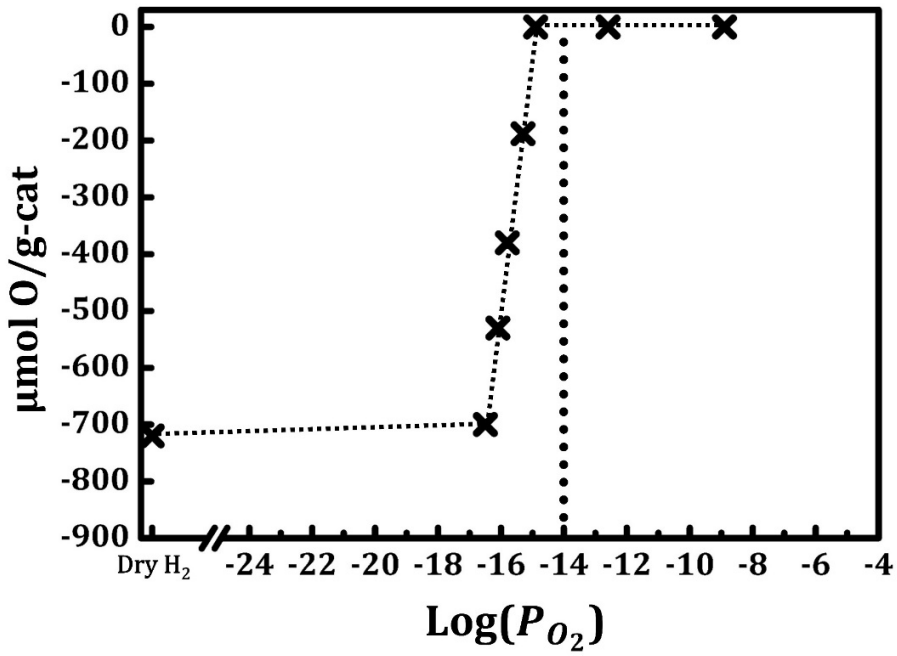

converted to NiO. The fact that the P_{O_2} remained constant during the oxidation process is consistent with equilibrium being established between Ni and NiO. The amount of oxygen required to completely oxidize the metallic Ni in coulometric titration agreed well with the value obtained in the flow-titration measurements in Table 1. Tabulated data for oxidation of bulk Ni would predict that the P_{O_2} should be 10^{-14} atm at 1073 K when both Ni and NiO are present in equilibrium. This is indicated by the dotted line in the plot. The difference between the measured P_{O_2} for the 5-Ni/MAO catalyst and tabulated data is relatively small but may be real. There are reports that the oxidation potential for a metal can shift to lower P_{O_2} with particle size due to the effects of surface energy [18] or interactions with the support [30]. The change in the equilibrium P_{O_2} with the extent of Ni oxidation could indicate that there is a distribution of environments for the Ni.

Figure 3a). Oxidation isotherm obtained using coulometric titration for 5-Ni/MAO at 1073 K (cross). The dotted line is the equilibrium value for bulk Ni.

Figure 3b). Oxidation isotherms obtained using flow titration for 5-Ni/LFO/MAO at 1073 K (black circle) and 973 K (red circle); results for LFO/MAO (triangle) were obtained using coulometric titration at 1073 K.

Results from equilibrium measurements for the 5-Ni/LFO/MAO and LFO/MAO samples are shown in Figure 3b) and Table 2. The data for LFO/MAO were obtained using coulometric titration at 1073 K. The amount of oxygen removed in coulometric titration agreed reasonably well with the reduction reported in Table 1. The small reduction of $LaFeO_3$ that is observed occurs at much higher P_{O_2} than that observed for Ni. Compared to 5-Ni/MAO, 5-Ni/LFO/MAO was significantly easier to oxidize and the data for this sample were measured using flow titration at 973 and 1073 K. To facilitate equilibration, the 5-Ni/LFO/MAO sample was first reduced in dry H_2 before exposing it to a flowing mixture of H_2 and H_2O corresponding to the

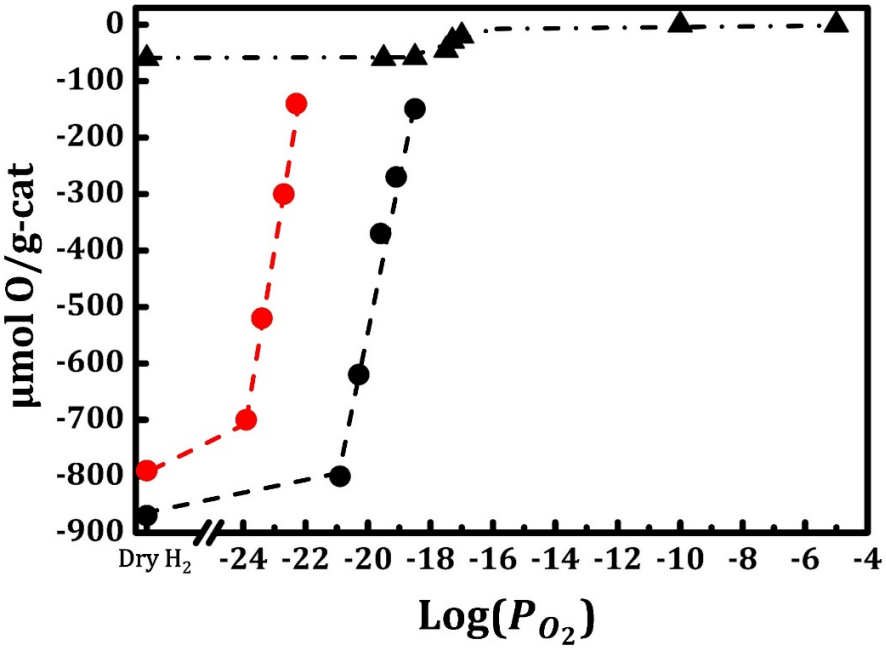

desired P_{O_2}. Pre-reduction for each data point ensured that Ni oxidation occurred by reaction with H_2O, in the presence of H_2, and was not due to sluggish kinetics for NiO reduction. Compared to bulk Ni, the equilibrium isotherm for Ni oxidation on 5-Ni/LFO/MAO at 1073 K

shifted to lower values of P_{O_2} by about 5 orders of magnitude. Furthermore, from the equilibrium constants at 973 and 1073 K and the thermodynamic identity in Equation (1), the oxidation enthalpy for 5-Ni/LFO/MAO was found to vary between 285 and 325±20 kJ/mol O_2, depending on the extent of reduction. This compares to the tabulated value of 280 kJ/mol O_2 for oxidation of bulk Ni at 1073 K.

$$\Delta H = \left\{ \frac{-R\delta \ln(K_{NiO})}{\delta\left(\frac{1}{T}\right)} \right\}_x \quad (1)$$

By itself, the change in ΔH is not sufficient to explain the five order-of-magnitude shift in K_{NiO}. The magnitude of -ΔS must also decrease, from 180 J/mol·K to 140 J/mol·K. A similar decrease in -ΔS was reported for oxidation of the mixed oxide, $Ce_yZr_{1-y}O_2$, compared to pure CeO_2 [27]. The authors of that study argued that the decreased entropy change was due to a decrease in the number of identical lattice positions that could accommodate the oxygen atoms of the mixed oxide. Similar arguments may explain the changes for Ni on the LFO/MAO support. If Ni was constrained at the surface, such as what would occur in a two-dimensional film, the possible locations for oxygen atoms would decrease.

Table 2. Flow-titration measurements of oxygen uptakes following equilibration of the fully reduced 5-Ni/LFO/MAO sample in flowing H_2O-H_2 environments.

H_2O content in H_2 (%)	Log(P_{O_2}) (atm)	µmol O/g uptake (Ni reduction extent %) (±20 µmol O/g)	
1073 K			
0	-∞	870	100%
5	-20.9	800	92%
10	-20.3	620	71%
20	-19.6	370	43%
30	-19.1	270	31%

45	-18.5	150	17%
973 K			
0	-∞	790	91%
3	-23.9	700	80%
5	-23.4	520	60%
10	-22.7	340	39%
15	-22.3	140	16%

3.3 Coke Tolerance

A previous study of Ni on $CaTiO_3/MgAl_2O_4$ demonstrated that the perovskite-supported catalyst exhibited extreme tolerance towards coking [10]. Samples heated in dry, flowing CH_4 at 1073 K for 12 h showed minimal carbon formation, while a reactor containing a more conventional $Ni/MgAl_2O_4$ catalyst showed large amounts of filamentous carbon. To determine whether the 5-Ni/LFO/MAO catalyst might also exhibit resistance to coking, this sample was also exposed to dry flowing methane at 1073 K for 12 h, after which the carbon content of the sample was determined by measuring the CO_2 removed in flowing air at 1073 K in the same reactor used for flow titration. Similar to the result for $Ni/CaTiO_3/MgAl_2O_4$, the amount of carbon deposited on the 5-Ni/LFO/MAO sample was small compared to that which formed on the 5-Ni/MAO catalyst, 2.2 ± 0.3 mmol C/g (less than 3-wt%) versus 26 ± 2 mmol C/g (30-wt%). Indeed, the amount of carbon that forms on the 5-Ni/LFO/MAO is so small that it may not even be associated with coking of the Ni component. Because small Ni particles have been shown to exhibit better tolerance to carbon formation [31], this anti-coking behavior could be caused, in part, by stabilization of small Ni particles on the $LaFeO_3$ support. However, previous work with Ni ex-solving from doped $La_{0.7}Sr_{0.3}TiO_3$ exhibited high carbon tolerances even with very large Ni particles [2].

3.4 Methane Dry Reforming

To determine how the support and redox properties might affect catalytic activities, the Methane-Dry-Reforming (MDR) reaction was investigated on the reduced 5-Ni/LFO/MAO and 5-Ni/MAO samples. To ensure that the catalysts were in a stable state, the catalysts were pretreated using 5 redox cycles with 10% O_2 and 10% H_2 at 1073 K. Both catalysts were in a reduced state prior to carrying out reaction, and the initial reaction conditions were chosen to be 5% CH_4 and 5% CO_2 in He. The steady-state conversions were measured after the system had stabilized for 2 h at each temperature point. While the 5-Ni/MAO behaved as a conventional Ni catalyst for this reaction, we found that it was not possible to operate the 5-Ni/LFO/MAO in a stable manner under differential reaction conditions. However, high rates could be achieved under integral reaction conditions. In Figure 4a), the methane conversion is plotted as a function of temperature for both catalysts, using a fixed Gas Hourly Space Velocity (GHSV) of 60000 $mL \cdot g^{-1} \cdot h^{-1}$ (100 mL/min total flow rate, 100 mg catalyst). On 5-Ni/LFO/MAO, rates were so high that conversions essentially reached equilibrium for the MDR reaction. The equilibrium conversions, which include consumption of CO_2 due to the Reverse Water-Gas-Shift reaction [32,33], were calculated and are shown in the plot. The reaction was also measured on the $LaFeO_3/MgAl_2O_4$, there was no activity observed.

To compare these rates to literature values, turnover frequencies (TOF) were calculated from estimates of the Ni dispersion obtained from XRD measurements of the Ni particle size. Based on the Scherrer equation, the average Ni crystallite size for 5-Ni/LFO/MAO was 10 nm, implying a corresponding dispersion of 12% [34]. The calculated TOF for 5-Ni/LFO/MAO at 923 K was then 79.8 s^{-1}, which was notably higher than the values reported on Ni supported on SiO_2 in the literature [35]. The estimated TOF at these conditions for 5-Ni/MAO, 30 s^{-1}, was similar to more similar to that reported for conventional Ni catalysts. The 5-Ni/LFO/MAO catalyst was also stable. As shown in Figure 4b), rates measured at 893 K were largely unchanged over a period of 10 h.

Figure 4a). CH_4 conversions for the MDR reaction measured over 0.1-g samples of 5-Ni/LFO/MAO (circle) and 5-Ni/ MAO (cross). The feed concentration was 5% each for CH_4 and CO_2 in He and the total flow rate was kept constant at 100 mL/min. Equilibrium conversions for the MDR reaction (diamonds) are also shown.

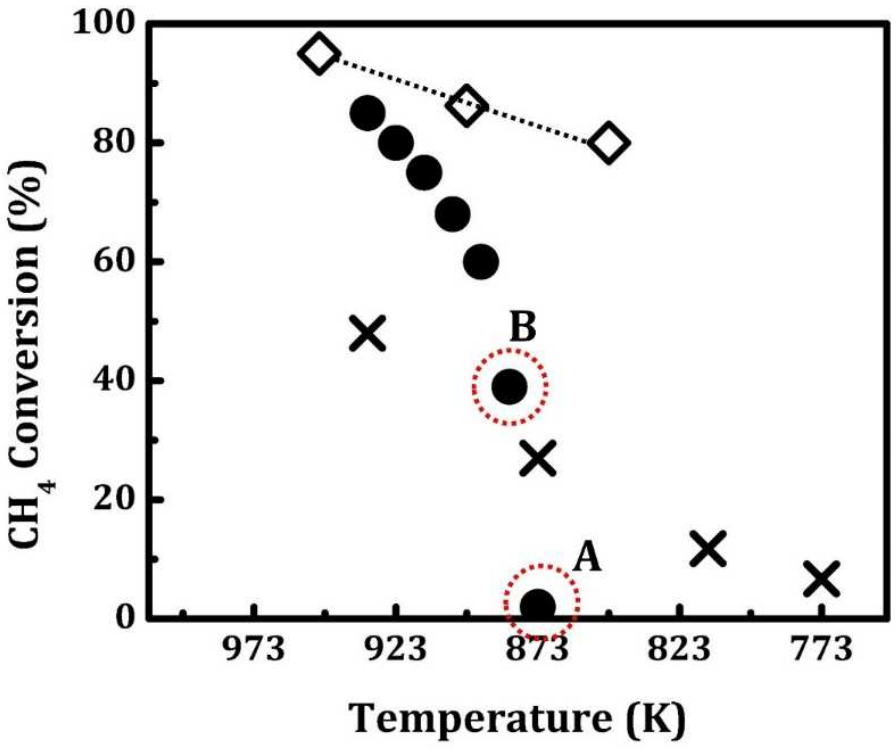

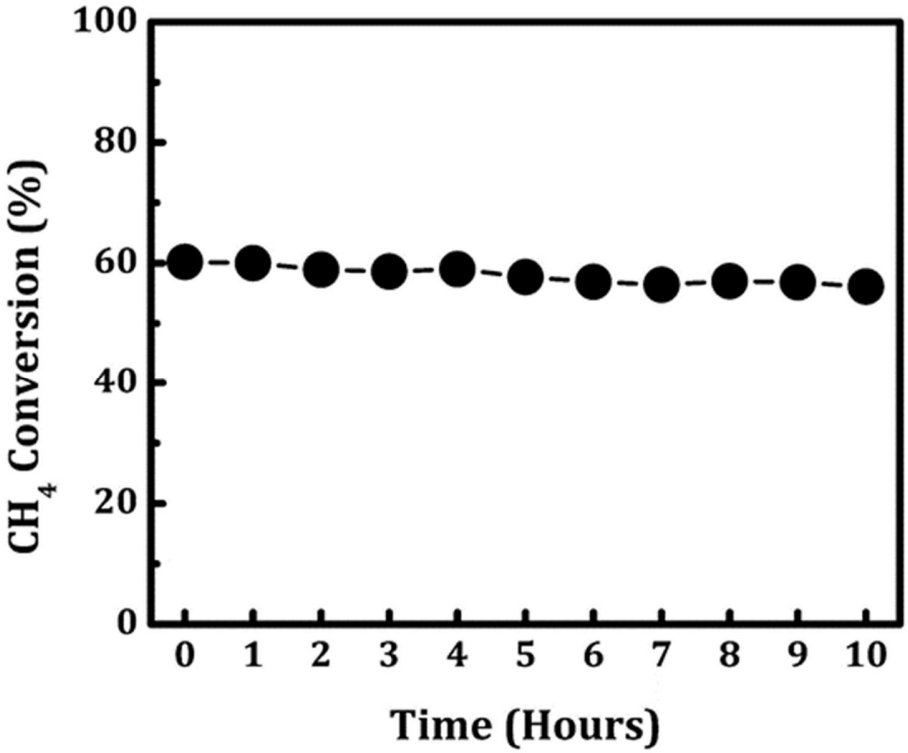

Figure 4b). CH_4 conversions for the MDR reaction measured over 0.1-g samples of 5-Ni/LFO/MAO at 893 K for 10 hours. The feed concentration was 5% each for CH_4 and CO_2 in He and the total flow rate was kept constant at 100 mL/min.

The data in Figure 4a) show a nearly stepwise transition from active to inactive states at approximately 873 K. It is important to note that this large change in activity was completely reversible upon changing the reaction temperature between 873 K and 923 K. The conversions reported in the plot were stable over the period of at least several hours and did not depend on whether the experimental condition was approached from the high- or low-temperature side, so that the large change in conversion between points marked A and B was not due to an irreversible process, such as coking or sintering of Ni particles. As discussed in the Experimental Methods section, it is important to recognize that correlations of the flow conditions in our tubular reactor indicate that mixing will be sufficiently large to allow the reactor to be treated as

a Continuous Stirred Tank Reactor (CSTR) [28]. This implies that all parts of the catalyst bed will be exposed to the product composition.

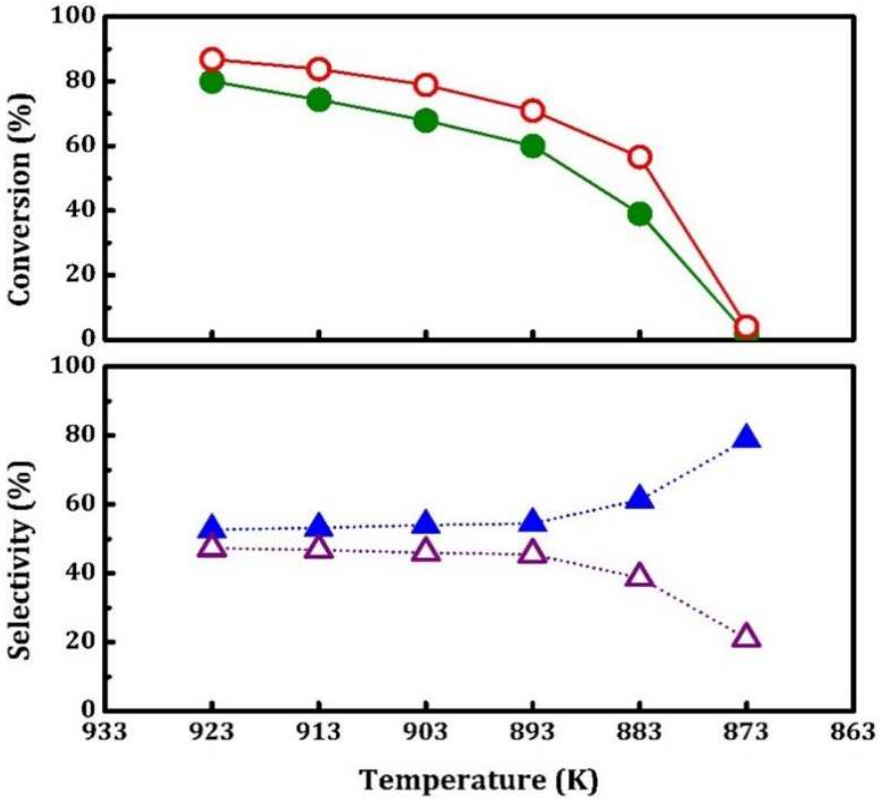

Figure 4c). Steady-state conversions of CH_4 (green) and CO_2 (red) for MDR over 0.1-g sample of 5-Ni/LFO/MAO, and the corresponding product distributions, CO (blue triangle) and H_2 (red triangle). The feed concentration was 5% each for CH_4 and CO_2 in He and the total flow rate was kept constant at 100 mL/min.

The following observations demonstrate that the dramatic drop in conversions on the 5-Ni/LFO/MAO sample at ~873 K is due to surface oxidation of the Ni. First, the equilibrium constant for Ni oxidation on this catalyst can be extrapolated from the measurements in Figure 3b) and Equation (1). Values for K_{NiO}^{-2} in the temperature range at which the rates showed a precipitous drop are reported in Table 3, using K_{NiO}^{-2} of $10^{-18.5}$ atm at 1073 K and -ΔH of 320 kJ/mol O_2. Table 3 also shows the P_{O_2} established by the reaction conditions, calculated from the

CO_2:CO ratio in the products, shown in Figure 4c), assuming equilibrium for $CO + \frac{1}{2}O_2 = CO_2$. Table 3 demonstrates that the conditions established by the reaction at points A and B in the plot are very close to the equilibrium conditions at which NiO should form. At higher temperatures, the P_{O_2} established by reaction are significantly lower than K_{NiO}^{-2}, which implies that the Ni should remain metallic. Second, additional evidence for deactivation being due to Ni oxidation came from the fact that, in the region of points A and B, small changes in the GHSV caused large changes in the conversions. For example, starting from point B, small increases in the total feed flow rate led to a precipitous drop in the conversion due to a decrease in the CO_2:CO ratio and subsequent deactivation due to oxidation of the Ni.

Table 3. The extrapolated K_{NiO}^{-2} for Ni oxidation on the 5-Ni/LFO/MAO samples together with the calculated P_{O_2} from the MDR reaction in Figure 4.

Temperature (K)	Extrapolated K_{NiO}^{-2} from thermodynamic data	*Calculated Log[P_{O_2}]* for the reaction conditions.
923	-24.0	-24.8
903	-24.8	-25.4
893	-25.3	-25.4
883	-25.7	-25.1
873	-26.2	-22.4

To provide additional evidence that the drop in activity at lower temperatures in Figure 4a) is due to Ni oxidation, the MDR reaction was performed at 873 K (the temperature of point "A" in Figure 4a)) while varying the CH_4:CO_2 ratio in the feed. For these experiments, the CH_4 partial pressure was fixed at 5% and the CO_2 partial pressure was decreased while maintaining a constant GHSV. As shown in Figure 5a), the catalyst was essentially inactive when the ratio of CH_4:CO_2 was 1, but the conversions of both reactants rapidly increased when the ratio was raised above approximately 1.67. At this point, the CO_2 conversion increased to 80%, leading to a

CO:CO_2 ratio of 5 and a P_{O_2} of $10^{-26.6}$ atm, a value just below the calculated equilibrium constant, K_{NiO}^{-2} = $10^{-26.2}$ atm, implying the Ni should exist in the metallic state. Because the conversion of CO_2 remained high with further increases in the CH_4:CO_2 ratio, the Ni catalyst remained metallic and catalytically active. Results from the complementary experiment are shown in Figure 5b). In this case, the temperature was fixed at 883 K (the temperature of point "B" in Figure 4a)) and the CO_2 partial pressure was increased while fixing the CH_4 partial pressure. For a CH_4:CO_2 ratio of 1, the conversions of both CH_4 and CO_2 are reasonably high. However, when the CO_2 partial pressure increased, the conversions, along with the CO:CO_2 ratio, decreased, falling to near zero at a ratio of 5. This is again consistent with Ni becoming oxidized with increasing CO_2:CH_4 ratio. If deactivation were due to coking, increasing the CO_2 concentration should stabilize the catalyst,

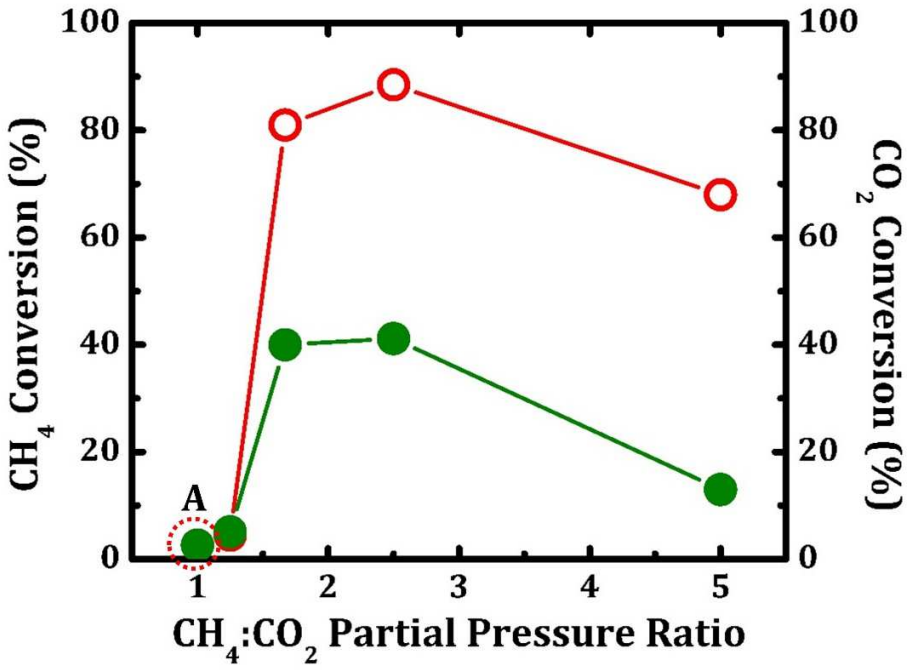

rather than cause deactivation.

Figure 5a). Steady-state conversions of CH_4 (green) and CO_2 (red) for MDR over 0.1-g sample of 5-Ni/LFO/MAO at 873 K. The total and CH_4 flow rates were fixed at 100 mL/min and 5 mL/min, respectively, while CO_2 flow rate was varied to adjust the CH_4:CO_2 ratio.

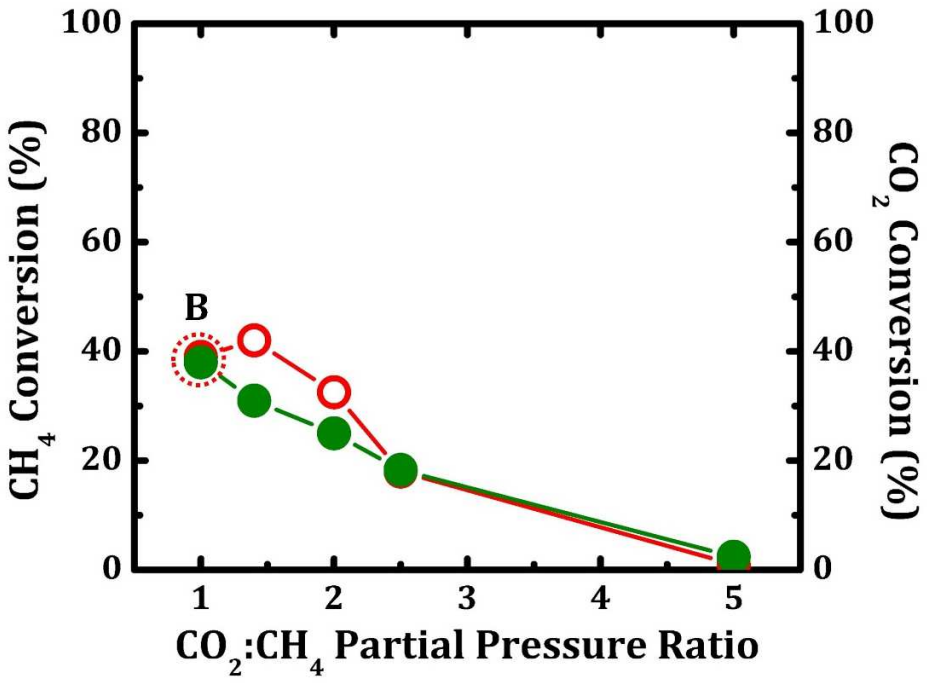

Figure 5b). Steady-state conversions of CH_4 (green) and CO_2 (red) for MDR over 0.1-g sample of 5-Ni/LFO/MAO at 883 K. The total and CH_4 flow rates were fixed at 100 mL/min and 5 mL/min, respectively, while CO_2 flow rate was varied to adjust the CO_2:CH_4 ratio.

It is important to notice that reaction rates in Figures 4 and 5 changed too rapidly for bulk oxidation or reduction of Ni. Steady-state conversions were established in just a few minutes, and the reactant flow rates were insufficient to add or remove the oxygen required to completely oxidize the Ni. Also, as shown in Table 1, complete oxidation of the Ni on the 5-Ni/LFO/MAO sample only occurred at higher temperatures in the flow-titration experiments. Therefore, the oxidation that is observed in the reaction experiments appears to be associated with surface Ni only. The fact that the equilibrium properties for surface Ni can be predicted from the bulk measurements is of additional interest.

4. Discussion

Most prior catalytic work on perovskite-supported metals has focused on the fact that metal dispersions can be maintained due to reversible ex-solution of the metal atoms into the perovskite lattice [1, 15, 36]. Far less attention has been given to the fact that strong interactions between the perovskite and the metal particles could alter other catalytic properties. While a number of groups have shown that perovskite-supported Ni can exhibit extreme tolerance against coke formation in the presence of dry methane [2, 3, 10], it has only recently been demonstrated that ex-solved metals can exhibit dramatically different properties for other reactions. Specifically, it was shown that Pt supported on $CaTiO_3$ thin films exhibited a higher activity for CO oxidation than Pt on non-interacting supports but was dramatically less active for hydrogenation of toluene [37]. The present study extends the observations of support effects to the thermodynamic properties of the metal. A major reason that the properties of perovskite-supported materials have not previously been investigated more thoroughly is that the perovskite surface areas tend to be low and an unknown fraction of the metal remains in the bulk of the perovskite, inaccessible to reactants [2, 14, 15, 38]. This has made comparisons between perovskite-supported metals with more conventional supported metals difficult.

In the present case, it is interesting to ask how contact with $LaFeO_3$ could so dramatically change the properties of Ni. In the absence of support migration to form overlayers on the metal catalyst (a phenomenon often referred to as Strong Metal Support Interactions (SMSI)) [39, 40], the effects of the support on the metal are not expected to extend more than a few atomic distances from the metal-support interface [41]. This would imply that the affected Ni in our study must essentially be in direct contact with the perovskite, since most of the Ni in three-

dimensional particles would be well separated from the support. This raises additional questions. If the Ni on $Ni/LaFeO_3/MgAl_2O_4$ is mostly present near the interface, why is it so difficult to oxidize the Ni at temperatures below 973 K? The difficulty in oxidizing the Ni suggests that there is a significant barrier to this oxidation, possibly associated with metal migration into the perovskite lattice. It is even more surprising that we observe rapid, reversible deactivation of catalyst activity, apparently due to Ni surface oxidation, at lower temperatures, ~873 K, upon only minor changes in the $CO:CO_2$ ratio. Finally, while it was very difficult to measure rates on the $Ni/LaFeO_3/MgAl_2O_4$ sample, it is clear that the catalyst was very active in its metallic state, showing conversions significantly higher than the conventional $Ni/MgAl_2O_4$.

It is noteworthy that the $Ni/LaFeO_3/MgAl_2O_4$ catalyst of the present study exhibited properties that were quite different from what was observed previously for $Ni/CaTiO_3/MgAl_2O_4$ [10]. Deactivation issues at differential reaction conditions were not observed in the $CaTiO_3$-supported materials and rates on activated catalyst were more similar to that of conventional supported Ni. This would imply that some perovskites influence metal catalyst properties more than other perovskites. This should not be surprising. Early ex-solution work showed that the not all catalytic metals can enter all perovskite lattices [7]. Similarly, based on experimental results and DFT simulations, Yanagisawa et al. reported that Pd showed very different chemical potentials for particle segregation when placed in either $LaFeO_3$ or $CaTiO_3$ [42]. At the time, results from those authors indicated much smaller differences for Pt in $LaFeO_3$ and $CaTiO_3$. This demonstrates that, even when a metal can ex-solve from two different perovskites, the thermodynamic properties and reducibility of the metal could still be quite different.

While the strong support effects observed in this study and the apparent differences between catalysts made with various perovskites supports certainly adds a level of complexity to

these catalysts, it also represents an opportunity that has not been fully explored. The potential to develop highly active catalysts with high stability against sintering and coking is certainly something that deserves additional study.

5. Conclusions

Thin $LaFeO_3$ films, deposited onto $MgAl_2O_4$ by ALD, are stable to redox cycling at 1073 K and can be used as catalyst supports for Ni. The presence of the perovskite films shift the thermodynamic equilibrium for Ni oxidation to significantly lower P_{O_2}. Ni supported on $LaFeO_3/MgAl_2O_4$ shows high activity for the MDR reaction and good tolerance against coking but deactivates due to Ni oxidation at low conversions.

Acknowledgements

This work was funded by the Department of Energy, Office of Basic Energy Sciences, Chemical Sciences, Geosciences and Biosciences Division, Grant No. DE-FG02-13ER16380. The STEM work was carried out in part at the Singh Center for Nanotechnology, part of the National Nanotechnology Coordinated Infrastructure Program, which is supported by the National Science Foundation grant NNCI-1542153. A.C.F. and E.A.S. acknowledge support to Integrated Mesoscale Architectures for Sustainable Catalysis (IMASC), an Energy Frontier Research Center funded by the U.S. Department of Energy, Office of Science, Basic Energy Sciences under Award # DE-SC0012573.

Declaration of Competing Interest

The authors declared that there is no conflict of interest.

References

[1] Y. Nishihata, J. Mizuki, T. Akao, H. Tanaka, M. Uenishi, M. Kimura, T. Okamoto, N. Hamada, Self-regeneration of a Pd-perovskite catalyst for automotive emissions control, Nature 418 (2002) 164-167.

[2] D. Neagu, T.S. Oh, D.N. Miller, H. Menard, S.M. Bukhari, S.R. Gamble, R.J. Gorte, J.M. Vohs, J.T.S. Irvine, Nano-socketed nickel particles with enhanced coking resistance grown in situ by redox exsolution, Nat. Commun. 6 (2015).

[3] P. Steiger, R. Delmelle, D. Foppiano, L. Holzer, A. Heel, M. Nachtegaal, O. Kröcher, D. Ferri, Structural reversibility and nickel particle stability in lanthanum iron nickel perovskite-type catalysts, ChemSusChem 10 (2017) 2505-2517.

[4] W.H. Kan, A.J. Samson, V. Thangadurai, Trends in electrode development for next generation solid oxide fuel cells, J. Mater. Chem. A 4 (2016) 17913-17932.

[5] Y.-F. Sun, Y.-Q. Zhang, J. Chen, J.-H. Li, Y.-T. Zhu, Y.-M. Zeng, B.S. Amirkhiz, J. Li, B. Hua, J.-L. Luo, New opportunity for in situ exsolution of metallic nanoparticles on perovskite parent, Nano. Lett. 16 (2016) 5303-5309.

[6] H. Tanaka, I. Tan, M. Uenishi, M. Kimura, K. Dohmae, Regeneration of palladium subsequent to solid solution and segregation in a perovskite catalyst: an intelligent catalyst, Top. Catal. 16 (2001) 63-70.

[7] H. Tanaka, M. Taniguchi, M. Uenishi, N. Kajita, I. Tan, Y. Nishihata, J. Mizuki, K. Narita, M. Kimura, K. Kaneko, Self-regenerating Rh- and Pt-based perovskite catalysts for automotive-emissions control, Angew. Chem., Int. Ed. 45 (2006) 5998-6002.

[8] K. Sutthiumporn, T. Maneerung, Y. Kathiraser, S. Kawi, CO_2 dry-reforming of methane over $La_{0.8}Sr_{0.2}Ni_{0.8}M_{0.2}O_3$ perovskite (M= Bi, Co, Cr, Cu, Fe): Roles of lattice oxygen on C-H activation and carbon suppression, Int. J. Hydrogen Energy 37 (2012) 11195-11207.

[9] Y. Kathiraser, W. Thitsartarn, K. Sutthiumporn, S. Kawi, Inverse $NiAl_2O_4$ on $LaAlO_3$-Al_2O_3: unique catalytic structure for stable CO_2 reforming of methane, J. Phys. Chem. C 117 (2013) 8120-8130.

[10] C. Lin, J.B. Jang, L.H. Zhang, E.A. Stach, R.J. Gorte, Improved coking resistance of "intelligent" Ni catalysts prepared by atomic layer deposition, ACS Catal. 8 (2018) 7679-7687.

[11] M. Seo, S.Y. Kim, Y.D. Kim, E.D. Park, S. Uhm, Highly stable barium zirconate supported nickel oxide catalyst for dry reforming of methane: from powders toward shaped catalysts, Int. J. Hydrogen Energy, 43 (2018) 11355-11362.

[12] T. Wei, L.C. Jia, H.Y. Zheng, B. Chi, J. Pu, J. Li, $LaMnO_3$-based perovskite with *in-situ* exsolved Ni nanoparticles: a highly active, performance stable and coking resistant catalyst for CO_2 dry reforming of CH_4, Appl. Catal., A, 564 (2018) 199-207.

[13] Y.J. Chai, Y. Fu, H. Feng, W.B. Kong, C.K. Yuan, B.R. Pan, J. Zhang, Y.H. Sun, A nickel-based perovskite catalyst with a bimodal size distribution of nickel particles for dry reforming of methane, ChemCatChem, 10 (2018) 2078-2086.

[14] K.J. Kim, H. Han, T. Defferriere, D. Yoon, S. Na, S.J. Kim, A.M. Dayaghi, J. Son, T.-S. Oh, H.M. Jang, Facet-dependent *in situ* growth of nanoparticles in epitaxial thin films: the role of interfacial energy, J. Am. Chem. Soc. 141 (2019) 7509-7517.

[15] S. Dai, S.Y. Zhang, M.B. Katz, G.W. Graham, X.Q. Pan, *In Situ* observation of Rh-$CaTiO_3$ catalysts during reduction and oxidation treatments by transmission electron microscopy, ACS Catal. 7 (2017) 1579-1582.

[16] T.M. Onn, M. Monai, S. Dai, E. Fonda, T. Montini, X.Q. Pan, G.W. Graham, P. Fornasiero, R.J. Gorte, Smart Pd catalyst with improved thermal stability supported on high-surface-area $LaFeO_3$ prepared by atomic layer deposition, J. Am. Chem. Soc. 140 (2018) 4841-4848.
[17] L. Adijanto, V.B. Padmanabhan, R.J. Gorte, J.M. Vohs, Polarization-induced hysteresis in CuCo-doped rare earth vanadates SOFC anodes, J. Electrochem. Soc. 159 (2012) F751-F756.
[18] E. van Steen, M. Claeys, M.E. Dry, J. van de Loosdrecht, E.L. Viljoen, J.L. Visagie, Stability of nanocrystals: thermodynamic analysis of oxidation and re-reduction of cobalt in water/hydrogen mixtures, J. Phys. Chem. B 109 (2005) 3575-3577.
[19] T. Kawasaki, J. Matsuda, Y. Tachikawa, S.M. Lyth, Y. Shiratori, S. Taniguchi, K. Sasaki, Oxidation-induced degradation and performance fluctuation of solid oxide fuel cell Ni anodes under simulated high fuel utilization conditions, Int. J. Hydrogen Energy 44 (2019) 9386-9399.
[20] M. Nurunnabi, Y. Mukainakano, S. Kado, B. Li, K. Kunimori, K. Suzuki, K.-i. Fujimoto, K. Tomishige, Additive effect of noble metals on NiO-MgO solid solution in oxidative steam reforming of methane under atmospheric and pressurized conditions, Appl. Catal., A 299 (2006) 145-156.
[21] S. Gaur, D.J. Haynes, J.J. Spivey, Rh, Ni, and Ca substituted pyrochlore catalysts for dry reforming of methane, Appl. Catal., A 403 (2011) 142-151.
[22] L.C. Buelens, V.V. Galvita, H. Poelman, C. Detavernier, G.B. Marin, Super-dry reforming of methane intensifies CO_2 utilization via Le Chatelier's principle, Science 354 (2016) 449-452.
[23] P. Wu, Y. Tao, H. Ling, Z. Chen, J. Ding, X. Zeng, X. Liao, C. Stampfl, J. Huang, cooperation of Ni and CaO at interface for CO_2 reforming of CH_4: A combined theoretical and experimental study, ACS Catal. 9(2019) 10060-10069.
[24] Z. Zhang, X.E. Verykios, Carbon dioxide reforming of methane to synthesis gas over Ni/La_2O_3 catalysts, Appl. Catal., A 138 (1996) 109-133.
[25] T. Onn, R. Küngas, P. Fornasiero, K. Huang, R.J. Gorte, Atomic layer deposition on porous materials: problems with conventional approaches to catalyst and fuel cell electrode preparation, Inorganics 6 (2018) 34.
[26] G. Zhou, P.R. Shah, T. Montini, P. Fornasiero, R.J. Gorte, Oxidation enthalpies for reduction of ceria surfaces, Surf. Sci. 601 (2007) 2512-2519.
[27] P.R. Shah, T. Kim, G. Zhou, P. Fornasiero, R.J. Gorte, Evidence for entropy effects in the reduction of ceria-zirconia solutions, Chem. Mater. 18 (2006) 5363-5369.
[28] O. Levenspiel, Chemical Reaction Engineering, 3rd Edition, John Wiley & Sons New York (1999) 309-311.
[29] J. Yoo, C.Y. Park, A.J. Jacobson, Determination of the equilibrium oxygen non-stoichiometry and the electrical conductivity of $La_{0.5}Sr_{0.5}FeO_{3-x}$, Solid State Ionics 175 (2004) 55-58.
[30] K. Bakhmutsky, N.L. Wieder, T. Baldassare, M.A. Smith, R.J. Gorte, A thermodynamic study of the redox properties of supported Co particles, Appl. Catal., A 397 (2011) 266-271.
[31] H.S. Bengaard, J.K. Nørskov, J. Sehested, B. Clausen, L. Nielsen, A. Molenbroek, J.R. Rostrup-Nielsen, Steam reforming and graphite formation on Ni catalysts, J. Catal. 209 (2002) 365-384.
[32] D. Pakhare, C. Shaw, D. Haynes, D. Shekhawat, J. Spivey, Effect of reaction temperature on activity of Pt-and Ru-substituted lanthanum zirconate pyrochlores ($La_2Zr_2O_7$) for dry (CO_2) reforming of methane (DRM), J. CO_2 Util. 1(2013) 37-42.

[33] S.T. Oyama, P. Hacarlioglu, Y. Gu, D. Lee, Dry reforming of methane has no future for hydrogen production: Comparison with steam reforming at high pressure in standard and membrane reactors, Int. J. Hydrogen Energy 37 (2012) 10444-10450.
[34] C.H. Bartholomew, R.J. Farrauto, Fundamentals of Industrial Catalytic Processes, 2nd Edition, John Wiley & Sons New York (2006) 86.
[35] J. Zhang, F. Li, Coke-resistant Ni@ SiO_2 catalyst for dry reforming of methane, Appl. Catal., B 176 (2015) 513-521.
[36] S. Zhang, M.B. Katz, S. Dai, K. Zhang, X. Du, G.W. Graham, X.Q. Pan, New atomic-scale insight into self-regeneration of Pt-$CaTiO_3$ catalysts: Incipient redox-induced structures revealed by a small-angle tilting STEM technique, J. Phys. Chem. C 121 (2017) 17348-17353.
[37] C.Lin, A.C. Foucher, Y. Ji, C.D. Curran, E.A. Stach, S. McIntosh, R.J. Gorte, "Intelligent" Pt catalysts studied on high-surface-area $CaTiO_3$ films, ACS Catal. 9 (2019) 7318-7327.
[38] T.S. Oh, E.K. Rahani, D. Neagu, J.T.S. Irvine, V.B. Shenoy, R.J. Gorte, J.M. Vohs, Evidence and model for strain-driven release of metal nanocatalysts from perovskites during exsolution, J. Phys. Chem. Lett. 6 (2015) 5106-5110.
[39] S. Tauster, S.C. Fung, Strong metal-support interactions: occurrence among the binary oxides of groups IIA–VB, J. Catal. 55 (1978) 29-35.
[40] S. Zhang, P.N. Plessow, J.J. Willis, S. Dai, M. Xu, G.W. Graham, M. Cargnello, F. Abild-Pedersen, X.Q. Pan, Dynamical observation and detailed description of catalysts under strong metal metal-support interaction, Nano. Lett. 16 (2016) 4528-4534.
[41] I. Ro, J. Resasco, P. Christopher, Approaches for understanding and controlling interfacial effects in oxide-supported metal catalysts, ACS Catal. 8 (2018) 7368-7387.
[42] S. Yanagisawa, A. Uozumi, I. Hamada, Y. Morikawa, Search for a self-regenerating perovskite catalyst using ab initio thermodynamics calculations, J. Phys. Chem. C 117 (2013) 1278-1286.

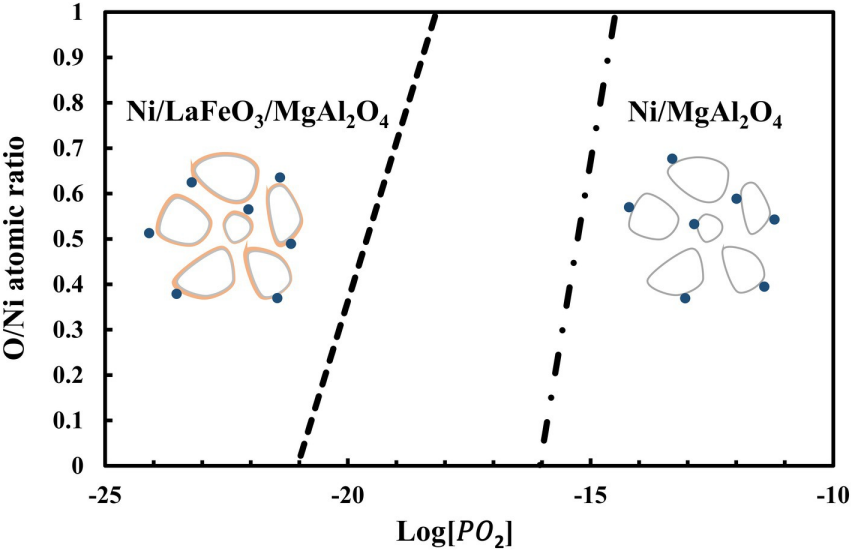
1
0.9
0.8
0.7
0.6
0.5
0.4
0.3
0.2
0.1
0
O/Ni atomic ratio
Ni/LaFeO3/MgAl2O4
Ni/MgAl2O4
-25
-20
-15
-10
Log[PO2]